


Article

Study on Shear Behavior and Mechanism Based on Shear Functional Unit of Loess Microstructure

Zhitao Hao ¹, Xi'an Li ^{1,2,*}, Rongrong Gao ¹, Wang Yao ³ , Yukun Wang ¹, Wenqi Zhao ¹ and Hongbo Sang ¹

¹ College of Geological Engineering and Geomatics, Chang'an University, Xi'an 710054, China; 2019026024@chd.edu.cn (Z.H.); 2020126103@chd.edu.cn (R.G.); 2022226103@chd.edu.cn (Y.W.); 2022126100@chd.edu.cn (W.Z.); 2022226089@chd.edu.cn (H.S.)

² Open Research Laboratory of Geotechnical Engineering, Ministry of Land and Resources, Xi'an 710054, China

³ School of Civil Engineering, Southwest Jiaotong University, Chengdu 610031, China; yaowangcdu@163.com

* Correspondence: dclixa@chd.edu.cn

Abstract: The structural specificity and hydrological sensitivity of loess have a strong impact on its long-term stability and safety. This topic is being actively researched and focuses on the macromechanical behavior of the shear strength of loess disturbed and its micromechanisms from the perspective of the dry–wet cycle (especially involving soluble salt erosion). In this paper, the correlation between micro-structural shear functional units and macroscopic degradation behavior was established by combining the changes in physicochemical properties of mass loss, surface cracking, strength deterioration, and structural disturbance of the loess with scanning electron microscopy (SEM) microscopic images in different dry–wet cycles and different salt contents. Results revealed that with the increase in dry–wet cycles and salt content, the mass loss of soil deteriorated and the surface crack rate increased. The cohesion of soil showed an overall decreasing trend, which decreased more obviously in the early stage of the dry–wet cycle, followed by a slow decrease, and tended to be constant after nine dry–wet cycles. However, the internal friction angle increased and then decreased during the whole cycle, and its value generally changed little. According to the deterioration and decay of shear strength, it can be concluded that the structural disturbance of loess increased with the increase in dry–wet cycles and salt content. At the same time, further linear quantization fitting of the structural disturbance parameters showed that the structural parameters had a positive correlation with salt content and a power function with dry–wet cycles, where dry–wet cycles seemed to play a dominant role in the loess structural deterioration rather than salt content. The microscopic study demonstrates that the dry–wet cycles and salt content do not directly affect the cohesion and internal friction angle of soil but change the basic shear structural unit of aggregate and then cause an essential impact on c and ϕ , which in turn have an essential impact on soil strength attenuation. This paper not only helps to elucidate the essence of water–soil–salt structural interactions but also provides theoretical references for sustainable development research in environmental engineering, geological engineering, and other related fields.

Keywords: dry–wet cycles; salt erosion; soil strength attenuation; structural disturbance; shear basic structural units



Citation: Hao, Z.; Li, X.; Gao, R.; Yao, W.; Wang, Y.; Zhao, W.; Sang, H. Study on Shear Behavior and Mechanism Based on Shear Functional Unit of Loess Microstructure. *Sustainability* **2023**, *15*, 11402. <https://doi.org/10.3390/su151411402>

Academic Editor: Md Mizanur Rahman

Received: 12 June 2023

Revised: 14 July 2023

Accepted: 19 July 2023

Published: 22 July 2023



Copyright: © 2023 by the authors. Licensee MDPI, Basel, Switzerland. This article is an open access article distributed under the terms and conditions of the Creative Commons Attribution (CC BY) license (<https://creativecommons.org/licenses/by/4.0/>).

1. Introduction

Loess is a wind-blown deposit in the Quaternary that covers large arid and semi-arid regions in mid-latitudes across the globe [1–3]. Loess fabric is mainly composed of skeleton particles or aggregates, which are dominated by clay, silt, sand, and soluble salt. The material composition, particle morphology, contact, and connection modes of loess are very complex [4,5]. In dry conditions, the cemented structure system with a certain strength is formed, and it is easy to lose its initial structural state when affected by humidification conditions [6,7]. Soil erosion caused by dry–wet alternation is the main form of soil degradation, and the alternation of dry and wet at different levels accompanied

by water migration creates the structural difference of loess [8]. This significantly affects the properties and quality of the soil, the productivity of the ecosystem, and the sustainability of environmental management, which leads to the failure of some large-scale constructions, the occurrence of natural disasters, and even the evolution of the global soil layer [9,10]. For example, dry–wet and saline weathering of slopes in the Loess Plateau region of China, severe salinization in agricultural irrigation areas, cracking and movement of landslides due to short-term rainfall or pumping irrigation, deterioration of soil infrastructure engineering properties, global soil water erosion degradation, etc. [11–15].

Because of this, many scholars have conducted fruitful studies on the physical and mechanical properties of loess under the alternating effects of drying and wetting [13,16]. It is discussed that the most important influence is the change in crack evolution, pore development, soluble salt dissolution, and cementation structure of the soil [17,18]. The development of pores and cracks and structural changes also lead to significant decay in the deformation modulus of loess, a gradual increase in permeability, air permeability, and compressibility, and irreversible changes in stress–strain relationships and water-holding properties [11,15,19,20]. These research results on loess properties and their influence mechanisms effectively guide engineering practice in loess areas and help us understand the mechanisms of the dry–wet cycle on the physical and mechanical properties of loess. Based on this observation, it is of great practical importance to carry out research on the changing pattern of the loess structure and strength (especially shear strength) under dry–wet cyclic conditions for the study of natural disasters due to dry–wet variations.

The dry–wet process is usually accompanied by the dissolution and clustering of salt crystals. Due to the open fabric structure and water-sensitive inter-particle bonds of loess, the phenomena of “salinization” and “salt bloom” often occur in the soil under the action of pressure and moisture increase or decrease [21]. It was also found that loess with salt was weakened by humidification, and the structure was softened after several cycles of dry–wet, which made the loess lose most of its strength [21,22]. Studies show that soluble salt is an important cement in the loose-structure systems of loess. It is generally believed that soluble salt plays a certain role in the cementation of loess only when the salt is very dry and crystalline. The dissolution of soluble salt will change the stable structure of loess, which will also cause changes in soil solubility, swelling, and permeability [23–26]. In addition, the dissolution of soluble salts can increase the type and concentration of ions in the soil and change the magnitude of the gravitational force between particles, thus directly affecting the structural strength and mechanical properties of the loess [27]. Therefore, although the connection between physical and mechanical properties of loess and dry–wet alternation is usually well established, it is still rare to study the intrinsic mechanism of shear parameters and structural changes in loess from the perspective of the dual action of dry–wet and soluble salt. Moreover, the combination of shear behavior characteristics of loess macro-structure and micro-structure shear functional units has not yet been reported to describe the process of loess shear behavior completely.

The macroscopic properties of loess and the microstructures of those minerals have a fundamental relationship [28]. The dry–wet cycles cause obvious damage to the surface loess and affect the macro stability of the loess structure. The resulting cracks gradually develop into the soil interior, changing the microstructure and creating microscopic cracks within the loess, which in turn causes essential changes in the basic structural units of the soil and the contact types of the soil particles. The use of scanning electron microscopy (SEM) can characterize the distribution types of microscopic fractures, the migration rules of salt particles, and the deterioration characteristics of contact surfaces more clearly and intuitively, and then allow us to study the evolution of loess microstructure and its correlation with macroscopic mechanical behavior [29–31].

Considering the number of dry–wet cycles and salt content as the background to this study, tests of macroscopic crack development, shear strength measurement, and structural-mechanism evolution of loess were carried out. Combining macro- and micro-scale perspectives, this paper systematically studies the influence mechanisms of dry–wet

cycles and salt on loess shear strength and shear basic structural units and describes the essential relationship and internal mechanism between the changes in loess strength and aggregate structural units to provide a useful reference for production, construction, and disaster prevention in loess areas.

2. Materials and Methods

2.1. Test Materials

The sample collection region is Chan he at 4 m in the central region of Shaanxi Province, China ($34^{\circ}27' N$, $108^{\circ}99' E$), as shown in Figure 1. The physical properties of the experimental soils are listed in Table 1. G_s is the grain density, W is the natural moisture content, W_l is the liquid limit, W_p is the plastic limit, and ρ_d is the dry density.

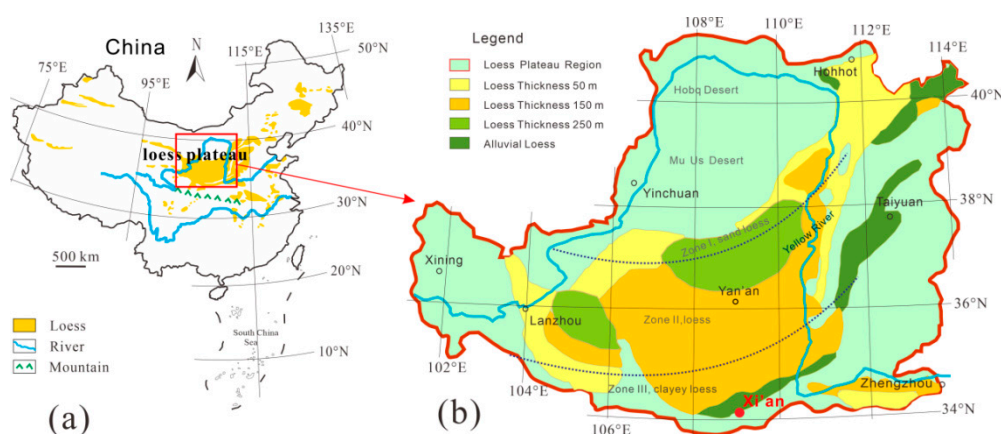


Figure 1. Loess map: (a) Loess distribution map of China; (b) Geological map of loess of loess plateau.

Table 1. Physical properties of the tested soils.

Particle Size Fraction (%)			W_L (%)	W_P (%)	G_s	ω (%)	ρ_d (g/cm ³)
>0.075 mm	0.075–0.005 mm	<0.005 mm					
2.78	73.06	24.16	29.12	17.50	2.70	16.92	1.41

2.2. Methods

2.2.1. Sample Preparation

Because sodium chloride is chemically stable, does not react with clay minerals, calcite, quartz, or air, and is a common component in natural groundwater, it is often chosen as the admixture salt in the dry–wet cycle [32]. The dried soil samples, after passing a 2 mm sieve, were added with not less than 99.5% sodium chloride produced by Tianjin Damao Chemical Reagent Factory. The mixture of soil and salt was fully stirred to ensure uniform mixing, which greatly promoted the experimental study of the influence of salt on soil engineering properties and was consistent with the idea of other scholars that salt is added to soil or pores to measure salinity by mixing thoroughly [33,34]. Set salt content S as a percentage of total soil salt at 7 levels of 0.0%, 0.3%, 1.0%, 1.5%, 2.0%, 2.5%, and 3.0% (indicated below as $S_{0.0\%}$, $S_{0.3\%}$, etc.). After standing for 24 h, the sample maker was used to make a sample with a bottom area of 30 cm², a height of 2 cm, and a dry density of 1.6 g/cm³ with a direct shear ring knife. The water content of the soil sample was controlled at 17.0%, which was close to the optimal water content of the soil (Figure 2a).

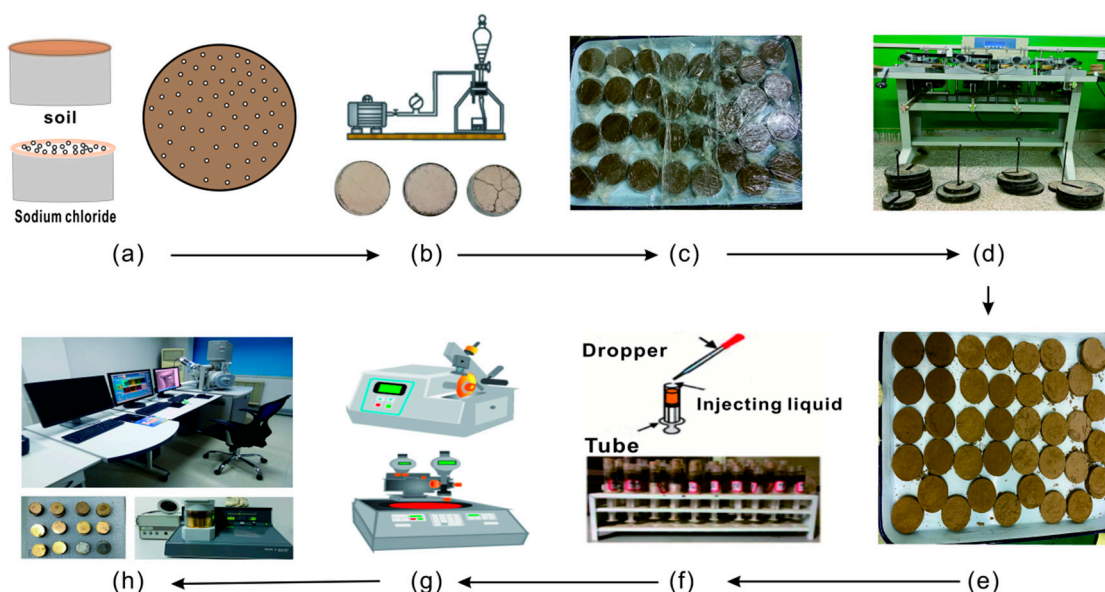


Figure 2. Sample preparation process: (a) Homogeneous mixing of soil with sodium chloride; (b) Process of dry–wet cycles; (c) Moisturization of samples; (d) Direct shear test; (e) Samples after shearing; (f) Gluing of microscopic samples; (g) Preparation of microscopic samples; (h) Testing of microscopic samples.

Previous studies have shown that the hydromechanical properties of loess change significantly at the beginning of the dry–wet cycle [35], and it has also been demonstrated that the engineering properties of loess do not change much in general after about 10 dry–wet cycles [16,36]. Therefore, the dry–wet cycle C is controlled as 0, 1, 2, 3, 6, 9, 12 (hereinafter denoted as C_0 , C_1 , etc.). The prepared ring knife samples were put into a vacuum saturator, and the samples were immersed in water (irrigation reflux) for at least 48 h, reaching a saturation greater than 97%, to simulate the infiltration of water [37–39]. The prepared saturated soil samples were then placed in an electric blast oven to simulate evaporation and dehumidification at a temperature of 30 °C for 12 h to bring the soil moisture content to a lower level close to zero. The above two steps as a dry–wet cycle process, humidification and dehumidification, continue until the completion of 12 dry and wet cycles (Figure 2b).

2.2.2. Direct Shear Test

Each ring-knife-dried sample to be sheared was sprayed after dehumidification with corresponding pure water uniformly to control its water content of 17.0% and immediately put into a sealed plastic bag for 24 h to moisturize it uniformly to ensure that the water content of the sheared specimen was consistent with the optimum moisture content of soil [21,39] (Figure 2c). The procedure was performed in a temperature/humidity-controlled room to reduce moisture exchange between the soil sample and the surrounding environment.

The direct shear test was performed according to the national geotechnical test standard (GB/SL 237-1999) [40], and the shear rate was set as 0.8 mm/min, the maximum shear amount as 6 mm, the shear duration as 4–5 min, and the vertical pressure as 100, 200, 300, and 400 kPa (Figure 2d,e).

2.2.3. Microscopic Test

To clearly understand the effects of dry–wet cycles and soluble salts on the hydraulic properties of soil samples from a micro-structural perspective. The microscopic sample preparation methods of Li and Li [41] and Li et al. [42] were used, and images were collected

by a Quanta FEG scanning electron microscope (SEM) for micro-structural experimental studies.

3. Results

3.1. Mass Strain Parameters of Soil Samples

The dry–wet cycle causes repeated dissolution and crystallization of soluble salts in the soil, resulting in repeated shrinkage and swelling of the soil, which also causes a loss of soil mass. In order to quantitatively describe the law of soil swelling and shrinkage deformation, a high-precision balance was used to measure the sample mass, and the variation law of sample mass caused by moisture increase and decrease was obtained (ignoring the loss of soil sample at the interface between soil sample and ring cutter). The mass strain parameter is used to reflect the mass loss rate [43]:

$$\Delta\epsilon_{m_{ij}} = (m_{0j} - m_{ij}) / m_{0j} \quad (1)$$

where $\Delta\epsilon_{m_{ij}}$ is the mass strain parameters of soil samples; m_{ij} is the mass of soil sample added with $j\%$ NaCl after the i -th dry–wet cycle; m_{0j} is the initial mass of soil sample added with $j\%$ NaCl without a dry–wet cycle.

Figure 3 shows the histogram of soil sample mass change under the dry–wet cycle and salt erosion. The mass strain parameter increases with the increase in salt content and the number of dry–wet cycles after several increasing and decreasing processes, from desiccation to saturation to redrying. After 1, 2, 3, 6, 9, and 12 cycles of dry–wet for soil samples with salinities of 0.0%, 0.3%, 1.0%, 1.5%, 2.0%, 2.5%, and 3.0%, the cumulative amounts of mass strain parameter increases are 0.0767, 0.0805, 0.0840, 0.0873, 0.0911, 0.0953, and 0.1001, respectively. This is because, on the one hand, soluble salt, medium salt, and sodium chloride crystals in soil are the first to dissolve due to the invasion of water, and the more cycles, the more severe the salt dissolution. On the other hand, the inclusion in the soil sample migrates with the migration of water and soluble salt, resulting in loose loss of cementing material, and the repeated dry–wet cycle also makes the soil skeleton subject to tensile force, which leads to the easier collapse and deformation of the soil with shrinkage and cracking. Therefore, the increase in both dry–wet cycles and salt content causes an aggravation in the loss of soil sample quality.

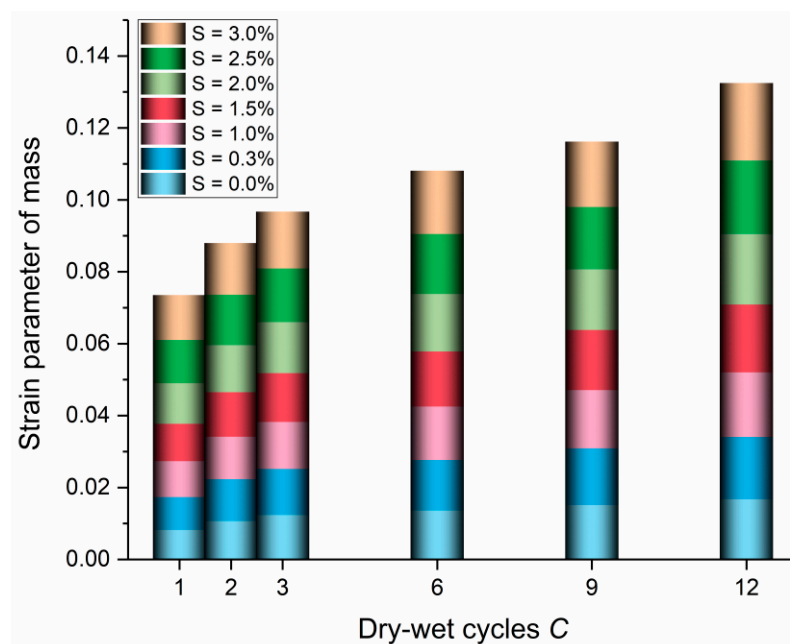


Figure 3. Variation pattern of mass–strain parameters of soil samples.

3.2. Surface Cracking and Crack Rate Variation

After dry–wet cycles and salt erosion, soil samples with different numbers of cycles and salt content have different deterioration characteristics on the surface. At the initial stage of humidification, water infiltrates into the surface layer of the ring-knife soil sample, and on the soil surface, soluble salts and gelling substances are first infiltrated, dissolved, and saturated. The subsequent infiltration of water does not further increase the saturation of the surface layer but advances to the interior of the soil sample with approximately the same saturation until it is fully saturated. In the process of dehumidification, the surface layer of the soil sample dehydrates and shrinks in volume. One or two fine crack lines first appear on the surface, especially on the appearance in contact with the ring cutter, which gradually lengthen and develop into main cracks, and a number of unevenly distributed small cracks are derived, resulting in overall shrinkage of the sample (shown as Figure 4a–d). After that, with the increase in the dry–wet cycle and sodium chloride content, the cracks become more obvious, and their width, depth, and number increase significantly (Figure 4e–h).

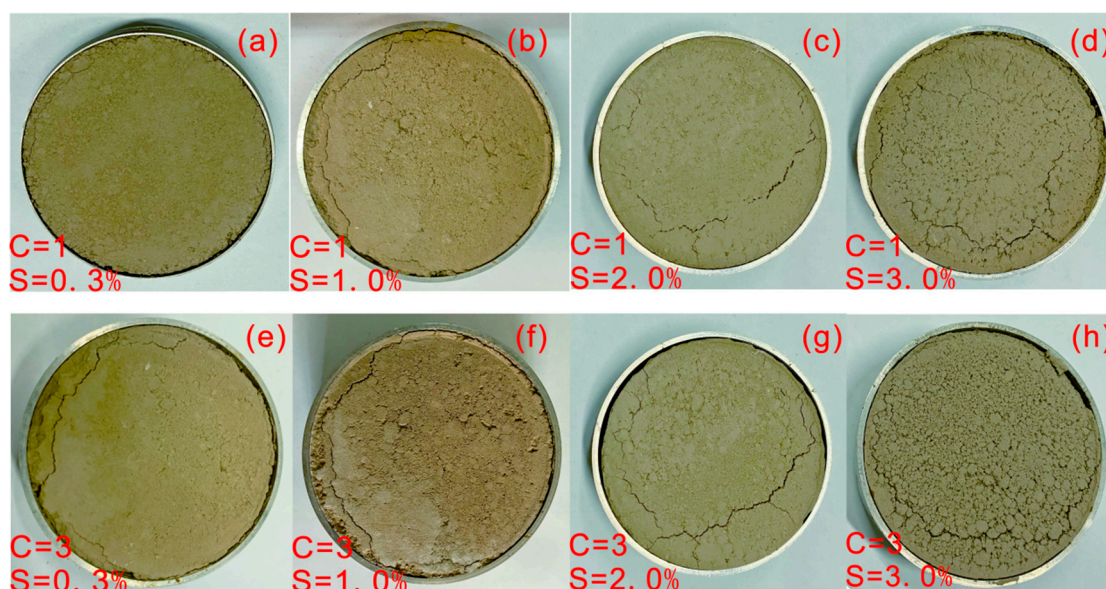


Figure 4. Surface crack development in soil samples: (a) 0.3% sodium chloride salt added; (b) 1.0% sodium chloride salt added; (c) 2.0% sodium chloride salt added; (d) 3.0% sodium chloride salt added; (e) 0.3% sodium chloride salt added; (f) 1.0% sodium chloride salt added; (g) 2.0% sodium chloride salt added; (h) 3.0% sodium chloride salt added (Where, (a–d) are samples with 1 dry–wet cycle, and (e–h) are samples with 3 dry–wet cycles).

In addition, we observe in the actual test that the surface of soil samples with high salt content forms white substances in the early dry–wet period. The generated white substances cover the surface of particles and aggregates in a large area or accumulate between aggregates (Figure 5). Hence, a comparative study on the cracking behavior of soil during the drying process shows that the development of macroscopic cracks is closely related to the number of dry–wet cycles and also closely related to the content of sodium chloride added. The measured surface crack rate can provide a quantitative and qualitative evaluation of the shrinkage characteristics of soil.

The particle and crack image processing system (PCAS) developed by Nanjing University was used to quantify the development of soil surface cracks [44]. The processing of a crack image consists of five steps: (i) To facilitate the comprehensive and accurate measurement of all surface cracks of the ring knife sample, a circular image is selected for data acquisition (Figure 6a). (ignoring the loss of part of the soil sample in contact with the ring knife during the dry–wet cycle); (ii) binarization treatment (Figure 6b); (iii) noise removal. Due to the presence of impurities in soil samples and the existence of some

“fake-areas”, errors will occur in the later quantitative analysis results, which must be removed in advance (Figure 6c); (iv) crack backbone extraction (Figure 6d); and (v) output the geometric and statistical parameters of the cracks (Figure 6e), including intersection point number, edge point number, end point number, total nodes, total line number, total crack area, and crack ratio. The surface crack rate R_{sc} is used as the crack measurement index.

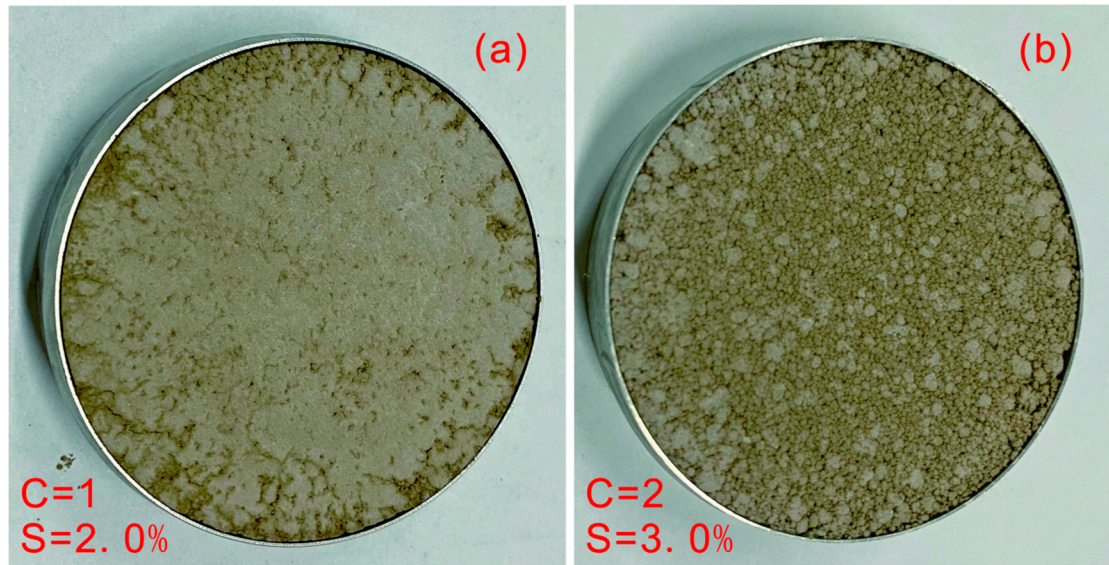


Figure 5. Salt crystallization adhesion phenomenon after soil dehumidification: (a) Samples were subjected to 1 dry–wet cycle with 2.0% sodium chloride salt; (b) Samples were subjected to 2 dry–wet cycles with 3.0% sodium chloride salt.

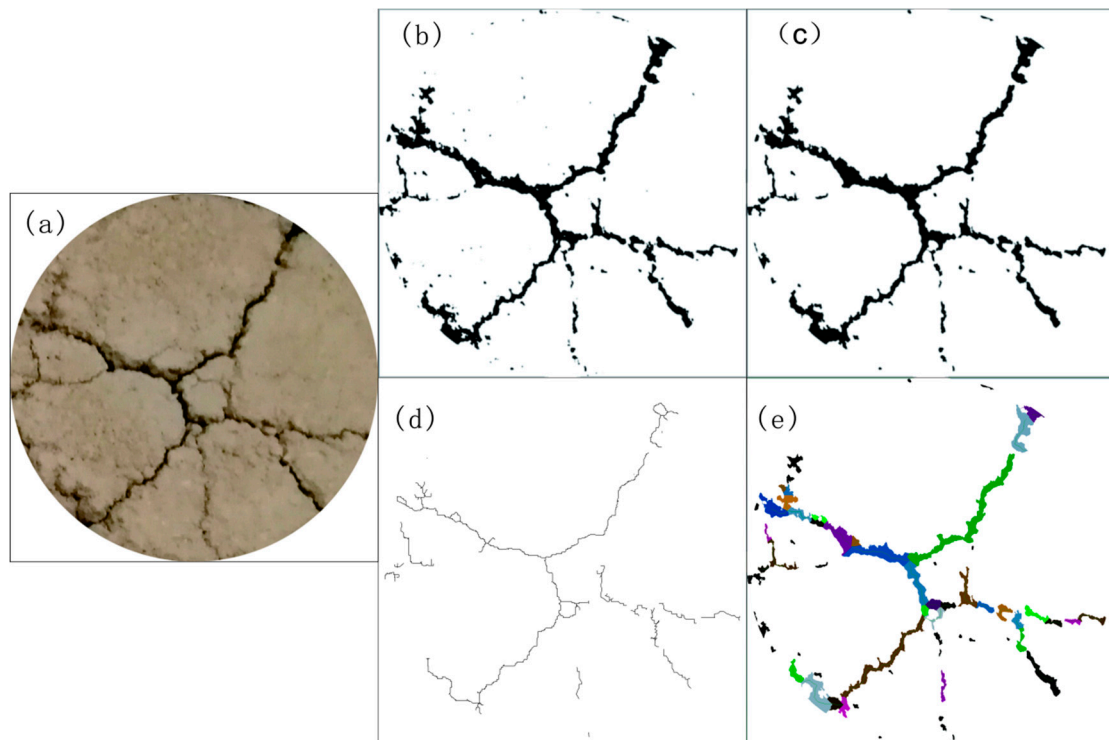


Figure 6. Crack image processing process: (a) Selected images; (b) Binarization treatment; (c) Noise removal; (d) Crack backbone extraction; (e) Crack identification and output data.

The surface crack rate is defined as the ratio of the crack area to the total area, which reflects the cracking degree of the soil [45].

$$R_{sc} = \frac{A_c^{sc}}{A^{sc}} \times 100\% \quad (2)$$

where A_c^{sc} is the surface crack area, and A^{sc} is the total area of the cross section of the soil sample.

Figure 7 shows the effect of dry–wet cycles on the surface crack rate of soil samples. On the whole, the surface crack rate increases with the increase in dry–wet cycles, but the variation law can be roughly divided into three gradients. In the first gradient, the soil sample undergoes initial saturation drying, and small cracks appear on the surface. After three cycles of dry–wet, the crack rate curve steepens rapidly, the soil cracks further develop, and the micro-cracks increase promptly. The crack curve of the second gradient shows a steady growth trend, which is due to the further extension of the original cracks and the continuous development of secondary micro-cracks in the process, and the total length and total depth of soil cracks increase significantly, which is the same as the results obtained by Tang et al. and Yin and Hu [46,47]. However, the crack rate curve in the third stage gradually slows down, indicating that the crack ratio at this time tends to be stable. Multiple dry–wet cycles experience a longer dry–wet process, where the water in motion dissolves more salts or forms colloids with some of these sticky particles and carries them out of their original position. After drying, the soil particles form a new skeleton and tend to the new uniform accumulation arrangement. Therefore, the test indicates that the loess crack rate tends to a steady state after nine dry–wet cycles.

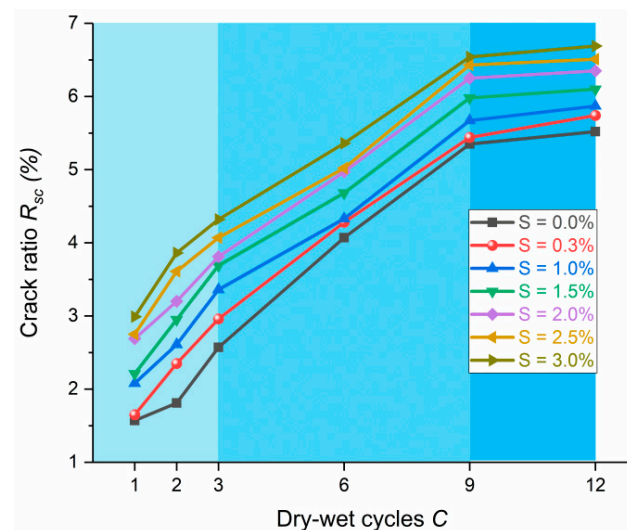


Figure 7. Effect of dry–wet cycles on the surface crack rate of soil samples.

The crack ratio of soil samples with different cycles increases with the increase in salt content (Figure 8). The reasons are as follows: On the one hand, when water molecules are in contact with the soil surface, the presence of surface salt leads to an enhancement of the soil's water absorption capacity. With the increase in salt content, the balance of electrostatic force in the soil is broken. Salt crystals are wrapped around the soil particles, and the soil particles gather together to form aggregates under the action of salt bonds, which makes the pores larger, the original cracks wider and deeper, and the new cracks appear. On the other hand, due to the formation of a certain thickness of hydration film in the outer layer of clay particles when they are hydrated, the spacing between particles is large in the saturation state, and the volume shrinkage and deformation are also large in the drying process, thus providing more space for the development of cracks [47].

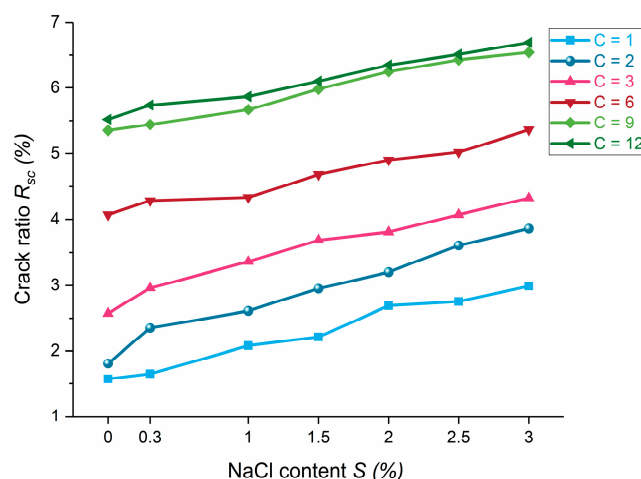


Figure 8. Effect of salt erosion on the surface crack rate of soil samples.

3.3. Shear Strength

Figure 9 shows the relationship curve between cohesion and dry-wet-salt erosion. It can be seen that the cohesion of soil samples decreases with an increase in dry-wet cycles and salt content. When C is equal to C_0 , the cohesion of soil decreases with the increase in salt content. The reason may be that the water bonds between soil particles are replaced by salt bonds due to the uniformly mixed salt, and the soil particles aggregate into coarser particles than the original ones [21]. The increase in salt crystal content leads to the formation of clusters, which leads to the full development of pores. In this case, the shear behavior is controlled by the shear failure of the aggregate clusters. Previous studies have found that the soil with larger aggregates is weaker than the soil with smaller aggregates, so the cohesion of the soil with larger aggregates is weakened [48,49].

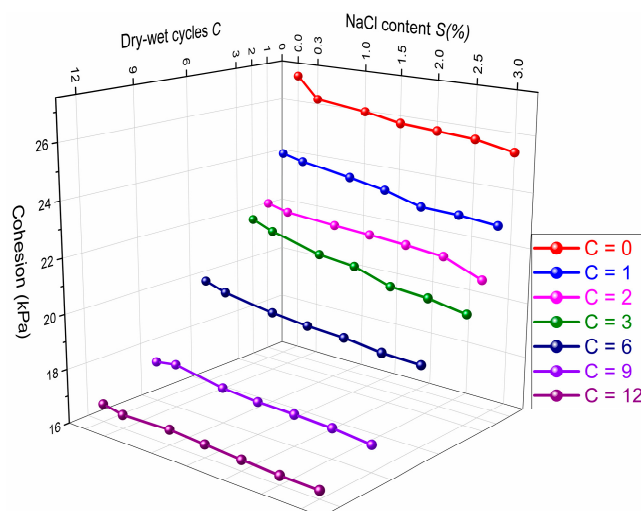


Figure 9. Variation in soil cohesion under dry-wet cycles and salt erosion.

Further observation can show that the decrease in cohesion is more obvious when C is equal to C_1 and C_2 . At the early stage of the dry-wet cycle, the soil is rapidly humidified. Clay particles and soluble salt between particles dissolve and leave their original positions, and then a new skeleton is formed after drying. That is, the initial dry-wet cycle greatly disturbs the soil and weakens its cohesion. It is worth noting that the soluble salt plays a significant role in the shear behavior [50]. The repeated dissolution of soluble salt in the wetting process and the re-precipitation after drying inevitably disturb the soil structure, enlarge the soil pores, and decrease the inherent cohesion. However, when $C \geq C_9$, the variation curves of cohesion with salt content tend to be stable. In particular, multiple dry-

wet cycles experience longer dry–wet processes. At this time, soil particles are more evenly arranged, the loess strength is more stable, and the cohesion is close to a constant value. Therefore, the dual action of salt and water changes the original cementation structure of soil and destroys the molecular gravitational force on the surface of particles, making the cohesive force lower.

The variation in the internal friction angle of soil under the action of dry–wet cycles and salt content is shown in Figure 10. The internal friction angle shows a trend of increasing at the beginning and decreasing at the end of the whole process, which shows little change in general. The reason is that the internal friction angle consists of inter-particle frictional force and inter-particle interlocking action [51]. The frictional resistance reflects the magnitude of the inter-particle friction, and the interlocking action is related to the roundness and structure of the inter-particle.

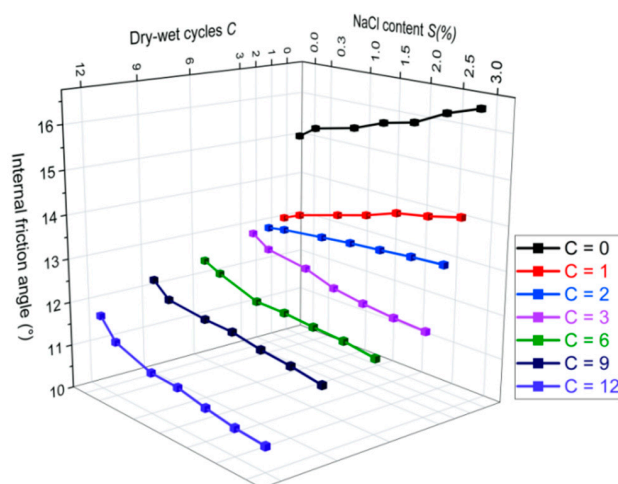


Figure 10. Variation in soil internal friction angle under dry–wet cycles and salt erosion.

When C is equal to C_1 and C_2 , the crystals formed by the soluble salts are not completely dissolved but wrapped on the surface of soil particles as the salt content increases. This makes the pore space between the particles decrease and the contact close, and the interlocking effect is enhanced. At the same time, salt consumes part of the bound water in the crystallization process, which makes the bound water film thin and the friction resistance strong [23]. Hence, the internal friction angle increases with increasing salt content. When $C \geq C_3$, there is a fundamental change in the internal friction angle to one that decreases with increasing salt content. The reason for this situation is that the number of salt crystals in the soil sample gradually decreases with the increase in the dry–wet cycles, and the inter-particle interlocking effect decreases, which decreases the number and strength of the cemented connections in the soil. In addition, the ability of soil particles to adsorb sodium ions progressively stabilizes, and the strong dispersion of sodium ions causes the particles to change from agglomeration to dispersion, which thickens the double electric layer around the soil particles. At this time, the water film between the particles becomes thicker, and the lubricating effect played by the water film weakens the frictional resistance and the shear strength of the soil.

4. Discussion

4.1. Relationships between Soil Structural Disturbance and Dry–Wet–Salt Erosion

The structural disturbance functions of soil samples are established based on the strain parameters of shear strength to investigate the relationship between the deformation characteristics of dry–wet–salt erosion under pressure and the structural disturbance parameters.

$$\Delta\tau_f = \frac{\tau_{f_{i0}} - \tau_{f_{ij}}}{\tau_{f_{i0}}} \quad (3)$$

where $\Delta\tau_f$ is the structure disturbance parameter based on shear strength, $\tau_{f_{ij}}$ is the shear strength of the soil sample supplemented with $j\%$ NaCl obtained by the i -th dry–wet cycle, and $\tau_{f_{i0}}$ is the initial shear strength without NaCl added obtained by the i -th dry–wet cycle.

The variation in soil structural disturbance parameters at different pressures is shown in Figure 11. The structural disturbance of shear strength increases with the number of dry–wet cycles and also grows gradually with the increase in salt content. C_3 seems to be a limit for the change of structural perturbation to occur. When $C < C_3$, the disturbance of soil structure is greatly influenced by both dry–wet erosion and salt erosion. Analysis of the reason: the dry–wet cycle directly affects the soil water distribution and also indirectly changes the bonding force in soil particles and the pore size, arrangement, and penetration. After the dry–wet cycle, the bond stress in soil particles is low, and the disturbance of soil structure is greater with the accumulation of crystallized salt. When $C \geq C_3$, the disturbance of soil structure increases steadily until flattening out, and the difference in soil structure disturbance increases with the increase in pressure. This indicates that the structural disturbance of soil is also affected by pressure. When the external force acts on the soil, it not only changes the arrangement and combination form of single and complex grains but also determines the transport and storage location of soil water and air and has a close relationship with the comprehensive characteristics of soil structure.

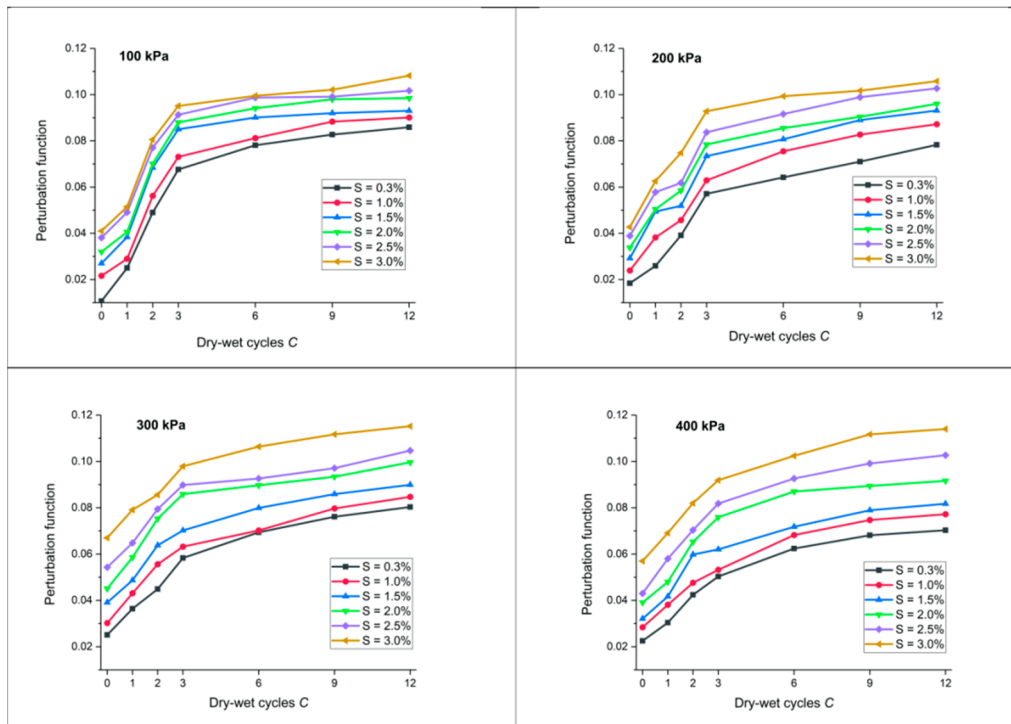


Figure 11. Disturbance function of loess structure under dry–wet–salt erosion.

A further univariate analysis of the soil structural disturbance parameters for dry–wet–salt erosion is conducted. By linear fitting of the structural disturbance parameters, the structural disturbance parameters of shear strength at different pressures have a certain regularity. It has a positive correlation with salt content and a power function relationship with the number of dry–wet cycles (as shown in Figure 12). The structural fitting equations of dry–wet–salt erosion and disturbance parameters are established.

$$m_{\tau_{fs}} = k_{s1} \cdot S + k_{s2} \quad (4)$$

$$m_{\tau_{fc}} = k_{c1} \cdot C^{k_{c2}} \quad (5)$$

where $m_{\tau_{fs}}$ is the structural parameter under the influence of salt content, S is the salt content, k_{s1} and k_{s2} are constant terms, and k_{s1} is related to the positive stress σ . With the gradual increase in pressure σ , the value of k_{s1} changes from 0.0117 to 0.0105, and the value of k_{s2} increases from 0.0072 to 0.0241. $m_{\tau_{fc}}$ is the structural parameter of the dry–wet cycle, C is the number of dry–wet cycles, and k_{c1} and k_{c2} are constant terms. When $0 < k_{c2} < 1$, the denominator of k_{c2} is even, and is inversely proportional to the normal stress σ . The larger σ is, the smaller k_{c2} is, and the farther it is from the horizontal axis of the fitted image.

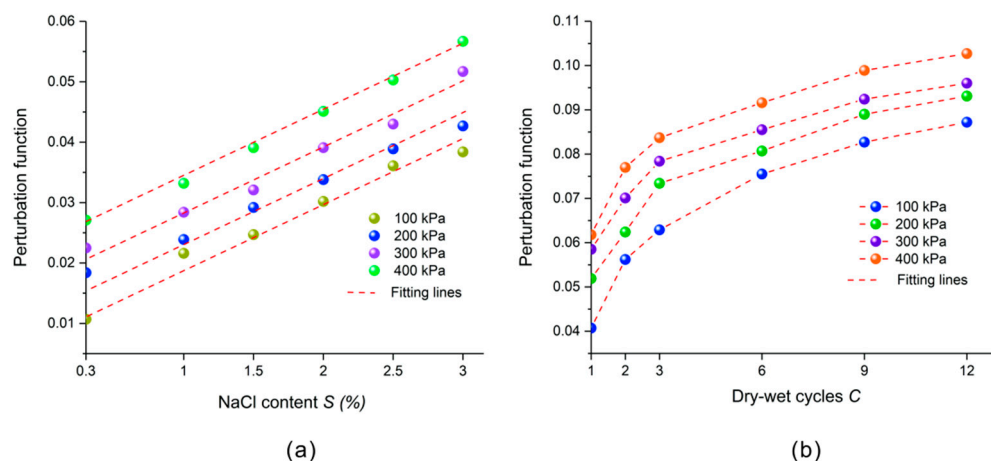


Figure 12. Fitting plots of structural disturbance parameters of soil shear strength: (a) The effect of salt content; (b) The effect of dry–wet cycles.

Figures 11 and 12 show that the structural parameters from C_1 to C_3 process increase rapidly. The reason is that while salt content influences structural parameters, the dry–wet cycle also plays a rapid catalytic role on structural disturbance parameters, and at this time the dry–wet cycle and salt erosion play a joint response. However, after 3–6 dry–wet cycles, the structural parameters gradually enter a flat state. A comparison with Figure 11 shows that the trend of structural parameters is similar to that in Figure 12b. It indicates that the number of dry–wet cycles seems to disturb the changing pattern of structural disturbance parameters significantly compared to the effect of salt content. When the influence of dry–wet cycles on soil structure disturbance is higher than that of salt content, it means that the dry–wet cycles play a dominant role in the deterioration process of loess structure rather than salt content.

4.2. Microstructural Analysis of Loess

4.2.1. Structural Difference of Loess Based on SEM Images

During the deposition and consolidation of loess, the aggregates formed by the bonding of soil particles are oriented in space, which is obviously different from the disturbed soil's structure. Comparing the scanning electron microscope (SEM) microstructures of loess that have undergone wet–dry–salt erosion (Figure 13), it can be seen that the increase in salt content and wet–dry times not only changed the initial relatively dense skeleton cementation of the loess into a loose structure separated and broken. It also reduced the number of micro and small pores and replaced them with an increased number of penetrating macropores and middle pores.

The dry–wet cycle and salt erosion cause disturbance, erosion, and even damage to the loess structure. However, the fundamental reason that the loess loses its original stability is that the structural units among the loess particles are destroyed. With the increase or decrease in moisture, the arrangement of particles in the basic structural units and the cementation mode of aggregates are changed and rearranged. The microstructure characteristics are expressed as many hollow structures and pores, and new structural units are formed (Figure 13 C_3 , C_6 and C_{12}). The increase in salts and salt concentration caused the salt bonds in the clay particles to replace the original water bonds, resulting in the

aggregation of particles into coarser sizes than clay, thus forming larger pore development structures (Figure 13a,b), which weakened the original shear resistance of soil [21]. This disturbance causes the soil skeleton to be stretched, the soil to contract and crack, and the formation of macro- and micro-cracks, which in turn leads to the formation of new basic structural units [38,52,53].

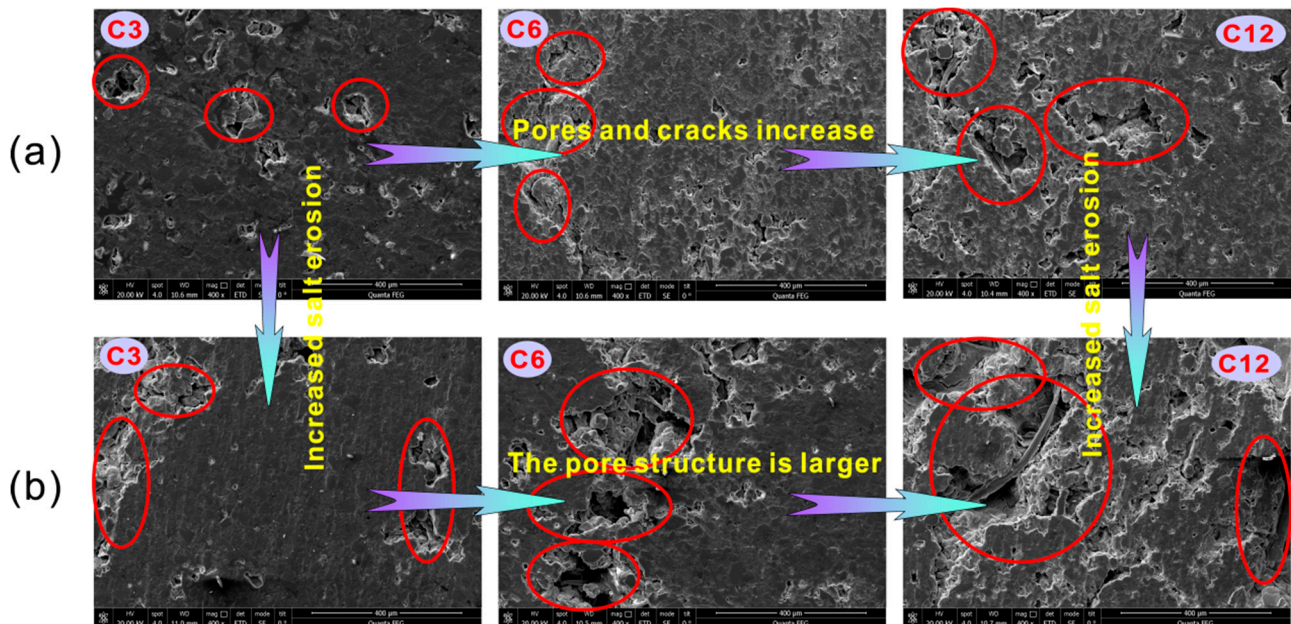


Figure 13. SEM of loess with 3, 6 and 12 dry-wet cycles: (a) 0.3% sodium chloride salt added; (b) 3.0% sodium chloride salt added (red area shows the change in pore erosion of soil samples under dry-wet-salt action).

4.2.2. Analysis of Microscopic Cracks

Repeated dry-wet-salt erosion enlarges the small cracks inside the soil, fractures the soil structure, and worsens the soil quality and geomechanical properties [50]. According to the size and shape of the cracks, the obvious microscopic cracks in Figure 14 can be divided into three categories: (i) banded connected crack (Figure 14a); (ii) banded semi-connected crack (Figure 14b); (iii) Annular semi-connected crack (Figure 14c). Through multiple dry-wet-salt erosions, the cracks continue to expand until multiple smaller cracks penetrate the soil structure. Resulting in the fragmentation of large aggregates and particles into smaller structural units, which forms more stable particle aggregates and stable structures of soil [54,55].

These cracks have a size effect and are regular. The segmentation of cracks is to divide the aggregate of fine sand particles into the aggregate of powder particles, and the adhesive particles wrapped around the powder particles are exfoliated, which makes the connection in the basic structural units of soil poor and extremely vulnerable to the erosion of external forces such as wind and water. A comparison of the EDS energy spectra in Figure 14 shows that the internal structure of the soil varies greatly. The main elements of soil are Si, Na, Ca, Al, and Mg, and the remaining K, Fe, Cu, and Zn content varies little. This indicates that dry-wet-salt erosion also has a large effect on the elemental content and its distribution inside the soil. The positions of various elements in loess pores are adjusted under microscopic hydrodynamic conditions. Although this adjustment does not result in material loss on the whole, it is of great significance to the microstructure and provides directions for our future research.

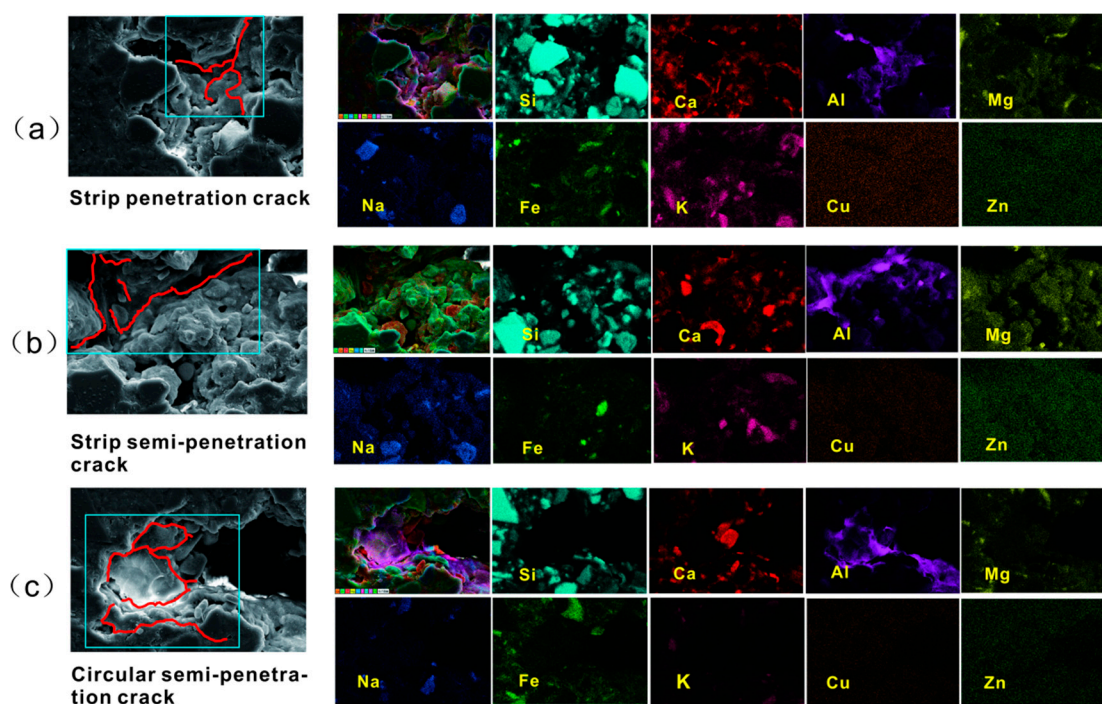


Figure 14. Internal microscopic cracks of soil samples and corresponding EDS elemental energy spectra: (a) 1.0% sodium chloride salt added; (b) 2.0% sodium chloride salt added; (c) 3.0% sodium chloride salt added.

4.3. Micro Mechanism Analysis of the Basic Shear Structural Units and the Shear Process of Loess

Increasing and decreasing moisture is bound to have an important impact on the distribution of the clay particles, colloidal particles, and even soluble salts in loess. The microscopic mechanism of this process is presented in Figure 15. As a result, on the one hand, the basic structural units of cementation are formed among the loess framework particles. On the other hand, the dissolution of salt crystallization and the dry–wet cycle can double erode the basic structural unit of soil, which makes the crystal surface of the skeleton mineral grains forming the main part of the pore wall smoother and the pore crack structure richer. Each dry–wet–salt erosion disturbance process restores the randomness of the clay distribution (and forms a more random erosion deterioration mechanism than the last disturbance). Therefore, the clay distribution around the disturbed loess skeleton particles is not uniform, and the strength of the new “sticky bridge” during the remodeling process is relatively weak.

The microstructure of loess, including particles, particle contact relationships, and cements, plays a key role in controlling the macroscopic mechanical behavior of loess [30]. The clay, silt, and salt of the soil are dissolved, migrated, and redistributed after increasing or decreasing moisture. The crystal surface of skeleton mineral grains in the main part of the pore wall is relatively rough due to the random distribution of clay grains, forming a new form of cementation connection [32]. These colloidal connections constitute the typical “core-clothes” structure in loess, that is, the basic structural units unique to loess (Figure 15).

These typical “core-clothes” structural units have very different shear forms under the action of the positive stress σ [56,57]. The skeleton particles that constitute the “core” part of aggregate do not fracture under low shear stress but undergo a certain deviation and torsion. At this time, the cementation material in the aggregate migrates and redistributes to form a new, stable structure. When the shear force increases to a certain degree and the skeleton particles fracture and break along the shear direction (Figure 16a). The shear forces also act on the “core” and “clothes” parts of the soil aggregates, and usually the large skeleton particles are deflected along the shear direction. The shear surface is generated in

the “clothes” region of the adhesive particles, where the scattered particles stack more compactly under the force of compression and the particle joints break or misshape (Figure 16b). When the shear force is applied to the “clothes” part, the strength of the soil’s basic unit is significantly lower, especially the soil samples that have been eroded many times by dry–wet–salt erosion and have larger and richer pore crack structures (including but not limited to the microcrack formed by erosion). Under shear stress, soil particles tumble and rotate, and the distribution direction of adhesive and clay particles changes with the direction of force. The friction between broken particles decreases rapidly. The macroperformance is that the soil unit is broken, and the shear strength decreases instantaneously (Figure 16c). Therefore, dry–wet–salt erosion does not directly affect the cohesion and internal friction angle of soil but changes the basic shear structural unit of aggregate and then causes an essential impact on c and φ .

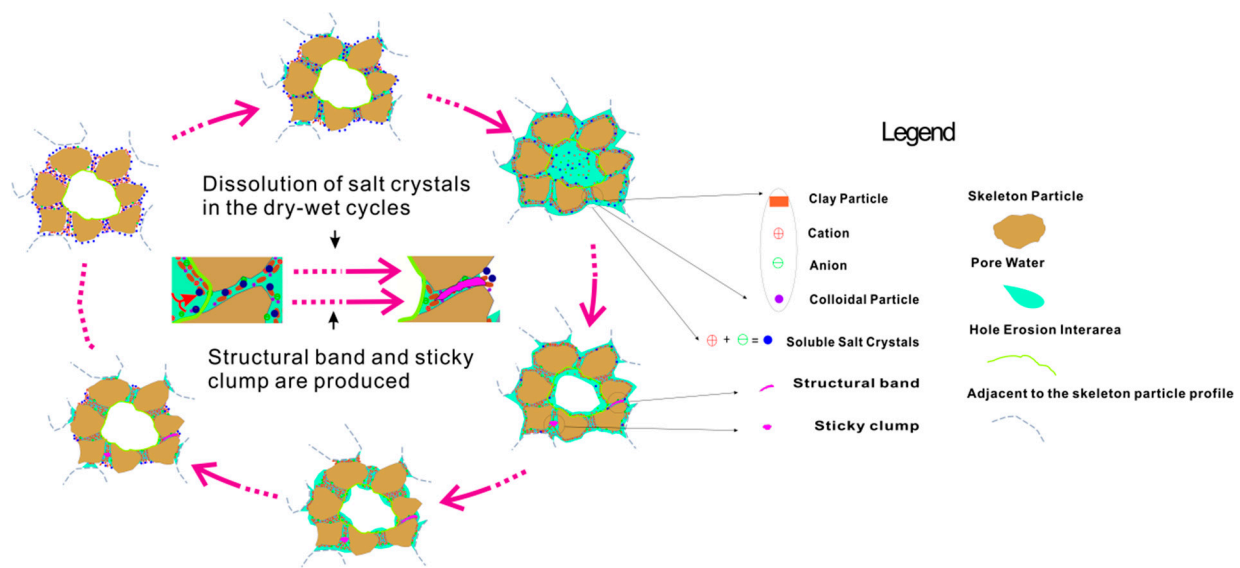


Figure 15. The conceptual model of the effect of dry–wet–salt erosion on the distribution of effective cementation between loess skeleton particles.

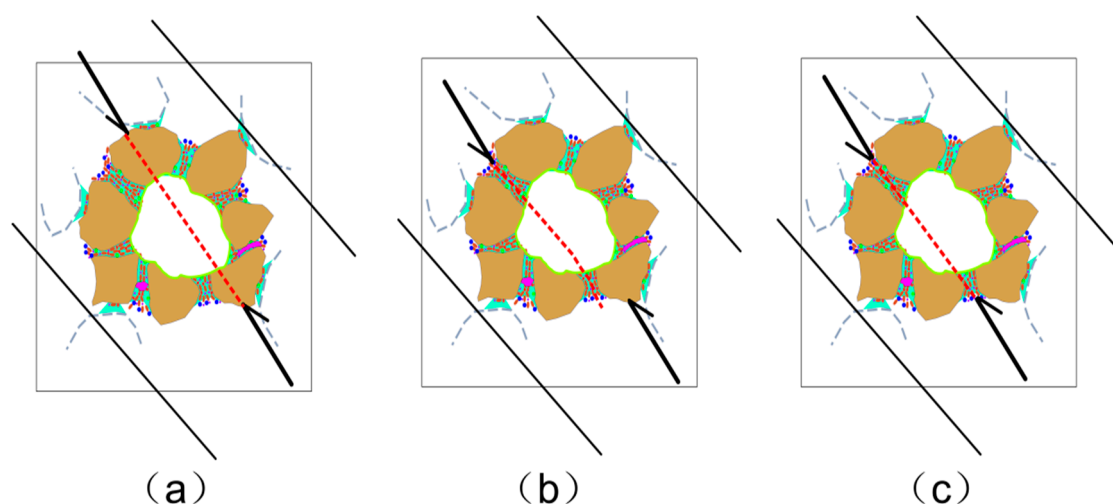


Figure 16. The basic structural unit shear types of loess: (a) Shear forces applied to the “core” of soil skeleton; (b) Shear forces applied to the “core-clothes” section; (c) Shear force applied to the “clothes” part; (the black arrow represents shear forces and the red dashed line represents the shear damage surface).

5. Conclusions

In order to elucidate how the nature of the soil's physicochemical properties changes with the dry–wet cycle and salt erosion, the study investigated the correlation between micro-structural shear functional units and the macroscopic deterioration behavior of the water–soil–salt interactions. The results are as follows:

- (1) The mass strain parameter effectively reflects the mass loss rate, and the increase in both dry–wet cycles and salt content causes an increase in the mass loss of soil samples.
- (2) The development of surface cracks in soil samples is closely related to the dry–wet-salt erosion. The surface crack rate can be used to qualitatively evaluate the shrinkage characteristics of soil and also quantitatively assess the development pattern of cracks as they increase with the increase in dry–wet cycles and salt erosion.
- (3) The dual effects of salt and water disturb the soil structure and change the original cementation structure, and the cohesion of soil samples shows an overall decreasing trend with the increase in dry–wet-salt erosion. While the internal friction angle shows a trend of increasing at the beginning and decreasing at the end in the whole process, which has little change in general.
- (4) A further univariate analysis of the soil structural disturbance parameters for dry–wet-salt erosion is conducted. The structural disturbance parameters have a positive correlation with salt content and a power function relationship with the number of dry–wet cycles.

The microstructure changes in loess shear basic structural units described in this study explain the mechanical behavior of dry–wet-salt erosion on loess shear strength and basic structural units and establish the fitting relationship between dry–wet-salt erosion and shear strength. Macro- and micro-analysis can provide technical support and theoretical reference to calculate the stability of loess disturbance in the Chan he areas. However, the relationship in this study must still be analyzed and verified in more detail in future research.

Author Contributions: All authors contributed to the conception and design of the study. Material preparation, data collection, and analysis were performed by Z.H., X.L. and R.G. The first draft of the manuscript was written by Z.H. and reviewed by X.L. The analysis was performed by R.G. and W.Y. The evaluation of the results was performed by Y.W., W.Z. and H.S. All authors commented on the manuscript. All authors have read and agreed to the published version of the manuscript.

Funding: This work was supported by the National Natural Science Foundation of China, grant number 42230712, the National Natural Science Foundation of China, grant number 41572264, and the National Natural Science Foundation of China, grant number 41877225. We are grateful to the anonymous reviewers and the Editors for their valuable comments, which have helped improve the quality of the manuscript.

Data Availability Statement: All data used in the study are confidential in nature, so the research data are not shared.

Conflicts of Interest: The authors declare no competing interest.

References

1. Pye, K. The nature, origin and accumulation of loess. *Quat. Sci. Rev.* **1995**, *14*, 653–667. [[CrossRef](#)]
2. Smalley, I.J.; Smalley, V. Loess Material and Loess Deposits: Formation, Distribution and Consequences. In *Developments in Sedimentology*; Elsevier: Amsterdam, The Netherlands, 1983; pp. 51–68. [[CrossRef](#)]
3. Yu, B.; Fan, W.; Dijkstra, T.; Wei, Y.; Deng, L. Pore structure evolution due to loess collapse: A comparative study using MIP and X-ray micro-CT. *Geoderma* **2022**, *424*, 115955. [[CrossRef](#)]
4. Song, Z.; Cheng, Q.; Zhang, W.; Meng, F. Analysis of microstructure and collapsibility of undisturbed loess. *J. Eng. Geol.* **2007**, *15*, 8. [[CrossRef](#)]
5. Sun, J. *Loess Science*; Hong Kong Archaeological Society: Hong Kong, China, 2005.
6. Derbyshire, E.; Mellors, T.W. Geological and geotechnical characteristics of some loess and loessic soils from China and Britain: A comparison. *Eng. Geol.* **1988**, *25*, 135–175. [[CrossRef](#)]
7. Grabowska-Olszewska, B. Skeletal microstructure of loesses—Its significance for engineering-geological and geotechnical studies. *Appl. Clay Sci.* **1989**, *4*, 327–336. [[CrossRef](#)]

8. Zhang, T.; Wang, X. Progress and trend of soil degradation research. *J. Nat. Resour.* **2000**, *15*, 280. [\[CrossRef\]](#)
9. Lal, R.E.; Blum, W.H.E.; Valentin, C.E.; Stewart, E. *Methods for Assessment of Soil Degradation*; CRC Press: Boca Raton, FL, USA, 1998.
10. Oldeman, L.R.; Hakkeling, R.T.A.; Sombroek, W.G. *World Map of the Status of Human-Induced Soil Degradation: An Explanatory Note*, 2nd ed.; International Soil Reference and Information Centre: Wageningen, The Netherlands, 1991.
11. Sorbino, G.; Nicotera, M.V. Unsaturated soil mechanics in rainfall-induced flow landslides. *Eng. Geol.* **2013**, *165*, 105–132. [\[CrossRef\]](#)
12. Wu, L.Z.; Zhou, Y.; Sun, P.; Shi, J.S.; Liu, G.G.; Bai, L.Y. Laboratory characterization of rainfall-induced loess slope failure. *CATENA* **2017**, *150*, 1–8. [\[CrossRef\]](#)
13. Xu, J.; Li, Y.; Wang, S.; Wang, Q.; Ding, J. Shear strength and mesoscopic character of undisturbed loess with sodium sulfate after dry-wet cycling. *Bull. Eng. Geol. Environ.* **2020**, *79*, 1523–1541. [\[CrossRef\]](#)
14. Xu, L.; Dai, F.C.; Tham, L.G.; Tu, X.B.; Min, H.; Zhou, Y.F.; Wu, C.X.; Xu, K. Field testing of irrigation effects on the stability of a cliff edge in loess, North-west China. *Eng. Geol.* **2011**, *120*, 10–17. [\[CrossRef\]](#)
15. Ye, W.J.; Li, C.Q.; Ma, W.C. Study on the mechanism of joint fissure development and expansion in Loess under the action of dry wet cycle. *Sci. Technol. Eng.* **2016**, *16*, 6. [\[CrossRef\]](#)
16. Xu, J.; Li, Y.; Ren, C.; Lan, W. Damage of saline intact loess after dry-wet and its interpretation based on SEM and NMR. *Soils Found.* **2020**, *60*, 911–928. [\[CrossRef\]](#)
17. Aldaoud, A.; Bouasker, M.; Al-Mukhtar, M. Impact of wetting-drying cycles on the microstructure and mechanical properties of lime-stabilized gypseous soils. *Eng. Geol. Amst.* **2014**, *174*, 11–21. [\[CrossRef\]](#)
18. Tripathy, S. Cyclic swell-shrink behaviour of compacted expansive soils. *Geotech. Geol. Eng.* **2008**, *27*, 89–103. [\[CrossRef\]](#)
19. Fu, L.; Li, M. Analysis of influence of dry wet cycle on permeability coefficient of undisturbed and remolded loess. *J. Luoyang Inst. Technol. Nat. Sci. Ed.* **2018**, *28*, 6.
20. Liu, J.Y.; Li, X.A.; Xue, Q.; Guo, Z.Z. Experimental study on air permeability and microscopic mechanism of intact and remolded Malan loess, Loess Plateau, China. *Bull. Eng. Geol. Environ.* **2020**, *79*, 3909–3919. [\[CrossRef\]](#)
21. Zhang, F.; Wang, G.; Kamai, T.; Chen, W.; Zhang, D.; Yang, J. Undrained shear behavior of loess saturated with different concentrations of sodium chloride solution. *Eng. Geol.* **2013**, *155*, 69–79. [\[CrossRef\]](#)
22. Barzegar, A.R.; Oades, J.M.; Rengasamy, P. Soil Structure Degradation and Mellowing of Compacted Soils by Saline-Sodic Solutions. *Soil Sci. Soc. Am. J.* **1996**, *60*, 583–588. [\[CrossRef\]](#)
23. Xu, H.L.; Gao, M.X.; Li, X.F.; Wang, Z.Y.; Liu, W.J.; Lu, Y. Study on influence of soluble salt concentration on shear strength index of soil. *J. Inn. Mong. Agric. Univ. Nat. Sci. Ed.* **2012**, *33*, 3.
24. Dijkstra, T.A.; Rogers, C.D.F.; Smalley, I.J.; Derbyshire, E.; Li, Y.J.; Meng, X.M. The loess of north-central China: Geotechnical properties and their relation to slope stability. *Eng. Geol.* **1994**, *36*, 153–171. [\[CrossRef\]](#)
25. Yan, Y.J.; Wen, B.P.; Huang, Z.Q. Effect of soluble salt on shear strength of Lanzhou unsaturated remolded loess. *Rock Soil Mech.* **2017**, *38*, 7. [\[CrossRef\]](#)
26. Zhang, N.; Luo, Y. Effect of soluble salt on strength characteristics of Loess. *Yellow River* **2014**, *36*, 3. [\[CrossRef\]](#)
27. Li, X.A.; Hong, B.; Li, L.C.; Wang, L. Experimental study on the influence of loess collapsibility on permeability coefficient. *China J. Highw. Transp.* **2017**, *30*, 12. [\[CrossRef\]](#)
28. Meng, J.; Li, X.A. Effects of carbonate on the structure and properties of loess and the corresponding mechanism: An experimental study of the Malan loess, Xi'an area, China. *Bull. Eng. Geol. Environ.* **2019**, *78*, 4965–4976. [\[CrossRef\]](#)
29. Liu, X.; Zhang, M.; Zhang, H.; Jia, Y.; Zhu, C.; Shan, H. Physical and mechanical properties of loess discharged from the Yellow River into the Bohai Sea, China. *Eng. Geol.* **2017**, *227*, 4–11. [\[CrossRef\]](#)
30. Shao, X.X.; Zhang, H.; Tan, Y. Collapse behavior and microstructural alteration of remolded loess under graded wetting tests. *Eng. Geol.* **2018**, *233*, 11–22. [\[CrossRef\]](#)
31. Wen, B.P.; Yan, Y.J. Influence of structure on shear characteristics of the unsaturated loess in Lanzhou, China. *Eng. Geol.* **2014**, *168*, 46–58. [\[CrossRef\]](#)
32. He, L. Control Law of Mineral Composition and Hydrochemical Composition on Shear Strength of Cohesive Soil and Its Application. Ph.D. Thesis, China University of Geosciences, Beijing, China, 2014.
33. Deng, Y.F.; Yue, X.B.; Cui, Y.J.; Shao, G.H.; Liu, S.Y.; Zhang, D.W. Effect of pore water chemistry on the hydro-mechanical behaviour of Lianyungang soft marine clay. *Appl. Clay Sci.* **2014**, *95*, 167–175. [\[CrossRef\]](#)
34. Dutta, J.; Mishra, A.K. A study on the influence of inorganic salts on the behaviour of compacted bentonites. *Appl. Clay Sci.* **2015**, *116*, 85–92. [\[CrossRef\]](#)
35. Wang, X. Study on Influence of Dry Wet Cycle on Shear Strength, Structure and Slope Stability of Loess. Master's Thesis, Xi'an University of Technology, Xi'an, China, 2017. [\[CrossRef\]](#)
36. Li, G.Y.; Wang, F.; Ma, W.; Fortier, R.; Mu, Y.H.; Mao, Y.C.; Hou, X. Variations in strength and deformation of compacted loess exposed to wetting-drying and freeze-thaw cycles. *Cold Reg. Sci. Technol.* **2018**, *151*, 159–167. [\[CrossRef\]](#)
37. Li, P.; Li, T.L.; Vanapalli, S.K. Vanapalli, Prediction of soil-water characteristic curve for Malan loess in Loess Plateau of China. *J. Cent. South Univ.* **2018**, *25*, 432–447. [\[CrossRef\]](#)
38. Lian, B.Q.; Wang, X.G.; Zhan, H.B.; Wang, J.D.; Peng, J.B.; Gu, T.F.; Zhu, R.S. Creep mechanical and microstructural insights into the failure mechanism of loess landslides induced by dry-wet cycles in the Heifangtai platform, China. *Eng. Geol.* **2022**, *300*, 106589. [\[CrossRef\]](#)

39. Sadeghi, H.; Hossen, S.B.; Chiu, A.C.F.; Cheng, Q.; Ng, C.W.W. Water retention curves of intact and re-compacted loess at different net stresses. *Jpn. Geotech. Soc. Spec. Publ.* **2016**, *2*, 221–225. [[CrossRef](#)]
40. SL237-1999; Industrial Standard of the People's Republic of China: Geotechnical Test Code. Ministry of Water Resources of the People's Republic of China: Beijing, China, 1999.
41. Li, X.A.; Li, L.C. Quantification of the pore structures of Malan loess and the effects on loess permeability and environmental significance, Shaanxi Province, China: An experimental study. *Environ. Earth Sci.* **2017**, *76*, 523. [[CrossRef](#)]
42. Li, X.A.; Li, L.C.; Song, Y.; Hong, B.; Wang, L.; Sun, J.Q. Characterization of the mechanisms underlying loess collapsibility for land-creation project in Shaanxi Province, China—a study from a micro perspective. *Eng. Geol.* **2019**, *249*, 77–88. [[CrossRef](#)]
43. Xu, L.N.; Deng, H.Y.; Niu, L.; Zheng, J.J.; Qian, Y.M. Experimental study on mechanical properties of fiber cement soil cured at low temperature under salt dry wet cycle. *J. Civ. Environ. Eng.* **2022**, *44*, 10.
44. Liu, C.; Tang, C.S.; Shi, B.; Suo, W.B. Automatic quantification of crack patterns by image processing. *Comput. Geosci.* **2013**, *57*, 77–80. [[CrossRef](#)]
45. Yin, J.; Hu, T. Mechanical properties of collapsible loess and effect of dry wet cycle on fissure development. *Yellow River* **2022**, *44*, 143–146. [[CrossRef](#)]
46. Lu, Z.H.; Chen, Z.H.; Pu, Y.B. CT study on the crack evolution of expansive soil during drying and wetting cycles. *Chin. Geogr. Sci.* **2002**, *23*, 417–422. [[CrossRef](#)]
47. Tang, C.S.; Shi, B.; Liu, C.; Wang, B.J. Factors affecting the surface cracking in clay due to drying shrinkage. *J. Hydraul. Eng.* **2007**, *38*, 8.
48. McDowell, G.R.; Bolton, M.D. On the micromechanics of crushable aggregates. *Géotechnique* **1998**, *48*, 667–679. [[CrossRef](#)]
49. Iverson, N.R.; Mann, J.E.; Iverson, R.M. Effects of soil aggregates on debris-flow mobilization: Results from ring-shear experiments. *Eng. Geol.* **2010**, *114*, 84–92. [[CrossRef](#)]
50. Kong, F.S.; Nie, L.; Xu, Y.; Rui, X.J.; He, Y.Y.; Zhang, T.; Wang, Y.Z.; Du, C.; Bao, C.H. Effects of freeze-thaw cycles on the erodibility and microstructure of soda-saline loessal soil in Northeastern China. *CATENA* **2022**, *209*, 105812. [[CrossRef](#)]
51. Qin, P.; Qin, Z. Study on the law of strength decrease of compacted fill with the increase of immersion time. *J. Zhejiang Inst. Water Resour. Hydropower* **2010**, *2*, 61–64. [[CrossRef](#)]
52. Shao, S.J.; Zhou, F.F.; Long, J.Y. Long, Structural properties of loess and its quantitative parameter. *J. For. Res.* **2004**, *15*, 243–245. [[CrossRef](#)]
53. Xie, D.; Qi, J. A new approach to the study of soil structure and its quantitative parameters. *Chin. J. Geotech. Eng.* **1999**, *21*, 651–656.
54. Tiwari, B.; Tuladhar, G.R.; Marui, H. Variation in Residual Shear Strength of the Soil with the Salinity of Pore Fluid. *Journal of Geotechnical and Geoenvironmental Engineering. J. Geotech. Geoenviron. Eng.* **2005**, *131*, 1445–1456. [[CrossRef](#)]
55. Wen, B.P.; He, L. Influence of lixiviation by irrigation water on residual shear strength of weathered red mudstone in Northwest China: Implication for its role in landslides' reactivation. *Eng. Geol.* **2012**, *151*, 56–63. [[CrossRef](#)]
56. Wang, S.; Xie, W.; Chang, Y.; Shan, S.; Jing, X. Study on microstructure and fractal characteristics of collapsible loess under water immersion. *Geol. J. Univ.* **2023**, *29*, 280–288.
57. Hao, Z.H.; Li, X.A.; Gao, R.R.; Hu, W.; Zhang, J.; He, J. Experimental study of the effect of bound water on the shear strength and structural units of Malan loess. *Q. J. Eng. Geol. Hydrogeol.* **2022**, *56*, qjeh2021-168. [[CrossRef](#)]

Disclaimer/Publisher's Note: The statements, opinions and data contained in all publications are solely those of the individual author(s) and contributor(s) and not of MDPI and/or the editor(s). MDPI and/or the editor(s) disclaim responsibility for any injury to people or property resulting from any ideas, methods, instructions or products referred to in the content.